The Medical Image Denoising Method Based on the CycleGAN and the Complex Shearlet Transform

ChunXiang Liu[1], Jin Huang[2], Muhammad Tahir[3,*], Lei Wang[4,*], Yuwei Wang[5], Faiz Ullah[6]
School of Resources and Environmental Engineering, Shandong University of Technology, Zibo, Shandong, China[1]
School of Computer Science and Technology, Shandong University of Technology, Zibo, Shandong, China[2, 4, 5]
Department of Computer Science, Mohammad Ali Jinnah University, P.E.C.H.S, Karachi, Sindh, Pakistan[3, 6]

***Abstract*—Medical image denoising plays an important role for the noise in the medical images can reduce the visibility, thereby affecting the diagnostic results of the doctors. Although good results have been achieved by the well-known deep learning-based denoising methods for their strong ability of learning, the loss of structural feature information and the well preservation of the edge information have not attracted considerable attention. To deal with these problems, a novel medical image denoising method based on the improved CycleGAN and the complex shearlet transform(CST) is proposed. The CST is used to construct the generator to embed more feature information in the training process and the denoising process is modeled to adversarial learn the mapping between the noise-free image domain and the noisy image domain. With the mechanism of the recurrent learning from the CycleGAN, the proposed method does not need the paired training data, which obviously speeds up the training and is more convenient than other classical methods. By comparing with five state-of-the-art denoising methods, experiments on the open dataset fully prove the accuracy and efficiency of the proposed method in terms of the visual quality and the quantitative PSNR, SSIM, and EPI.**

Keywords*—Medical image; image denoising; CycleGAN; complex shearlet transform

I. INTRODUCTION

Medical imaging techniques play the vital role in modern disease diagnosis, for they are the disruptive tools to observe the internal structure and functional information of human body. For example, the computed tomography(CT) can show the clear structure of the fracture [1] and the PET can effectively detect and distinguish the cancer or the normal metabolism of the of lung [2]. Though great success has been achieved, the main challenge comes from the possible noise or artifacts during imaging procedure, which may result in the unexpected diagnostic errors, even the death. For example, the noise will largely affect the results of image reconstruction [3]. Thus, the effective denoising methods are highly needed to be the fundamental and mandatory step of the medical imaging pre-processing or the further applications.

Nowadays, many advanced denoising methods have been proposed, all of which can be generally divided into four categories: the filter-based methods [4], the model-based methods [5], the multi-scale geometric transform-based methods [6] and the deep learning-based methods [7, 8]. For the filter-based methods, they typically implement the low-pass filters to replace the noisy or suspected pixel by their locally averaging value or energy in the neighboring region. The Gaussian filter, median filter and diffusion filter are the common methods in the early days. However, these methods are easy to produce the results with low contrast. Then, the bilateral filter [9], non-local filter [10], guarding filter [11], the block matching and 3D collaborative filtering (BM3D) [12] are successively proposed. They improve the denoising results, but are limited to the great diversity of the noise and the setting of the parameters, such as the height and width of the searching window. The model-based methods treat the denoising process to be a special mathematical model, for example, G. Gilboa et al. proposed to use the partial differential equations to describe the evolution of an image in time, and the solution of these equations are adapted to remove the noise and preserve the details [13]. Usually, the good results can be obtained, but the computational complexity is too high to implement in the real time application.

In recent years, for the low computational complexity and the superior properties in the frequency domain, a large number of work under the multi-scale geometric transform-based methods have been popularly reported, which decompose the noisy images into multi-resolution and different directions in each scale and then do the operations on the coefficients by the threshing scheme, considering the correlation of them, or the combination with the filters. According to the proposed time, the commonly used decomposition tools include the wavelet transform, curvelet transform, contourlet transform, non-subsampled contourlet transform, shearlet transform, non-subsampled shearlet transform [14, 15]. For example, A. Halidou et al. reported a new review on the wavelet transform based medical image denoising methods, which compare the performance of the typical wavelet, such as the discrete wavelet, Harr wavelet, and Dual-Tree complex wavelet [16]. P. S. Negi and D. Labate proposed a novel denoising method based on the discrete shearlet transform for CT images [17] and X. He et al. proposed the medical image denoising methods based on the non-subsampled version of the shearlet transform [18]. They decompose the input image into sub-images with different frequency bands and perform the denoising process for each sub-image separately, and then recompose the denoising sub-images into the results. It not only has good denoising effect and fast speed, but also has strong robustness, and can be applied in practical scene. A very good review of the multi-scale geometric transform-based methods on different image modalities can be found in [19, 20]. The benefits of the multi-

scale geometric transform-based methods are obvious since the features can be easy to capture in different scales, but they usually suffer from the disadvantages that the operations on the transformed coefficients may not match the distribution of the specific noise in different scales and directions. Though some typical models are proposed to alleviate the drawback, such as the generalized Gaussian distribution model in the wavelet and shearlet domain [21, 22], the Hidden Markov Model in the wavelet, NSCT and shearlet domain [23-25], Gaussian scale mixture model [26], the results are still not satisfying.

With the great breakthrough of the deep learning theory, it has been popularly applied in the medical imaging processing domain, such as the image U-net model for the super-resolution [27], the convolutional long short-term deep network for recognition of human action [28], and the graph resnet for motor imagery classification [29], as well as the image denoising. For example, K. Zhang et al. construct the "FFDNet" model for image denoising based on the conventional neutral network [30], W. Li et al. proposed to use the fast and flexible deep convolutional neural network(FFCNN) to remove the Gaussian noise [31] and K. Zhang et al. designed beyond Gaussian denoiser by the residual learning of deep CNN [32]. R. S. Thakur et al. compared the different performance of the state-of-art image denoising methods using convolutional neural networks in [33]. Recently, the good denoising results have been obtained by the generative adversarial network (GAN) model for it models the denoising task to be the game between the noisy image and denoising image, which is implemented by the learning strategy on the generative and the discriminator network [34]. Furthermore, to suppress the influence of the diversity of the noise and control the sampling variables, the conditional generative adversarial networks (CGAN) is proposed for removing the noise of the low-dose CT images [35]. The deep learning-based methods outperform the other methods for their strong representation and generalization ability of the deep level features. Though great success has been achieved, the deep learning-based methods also suffer from some obstacles, such as the large amount of training data, the selection of the pooling functions for the specific model and the unpredictable interpretability of the deep features.

On the other hand, comprehensively considering the advantages and disadvantages of the above methods, simultaneously using the multiscale feature and the deep features may be a good way to deal with their drawbacks. Very recently, some impressive works have been reported in this domain. For example, Z. Lyu et al. constructed the "NSTBNet" model based on the non-subsampled shearlet transform and a broad convolutional neural network to remove spatially variant additive Gaussian noise [36], C. Gu et al. combine the GAN and LSTM models for 3D reconstruction of Lung Tumors from CT Scans[37], Q. Song et al. proposed the multimodal sparse transformer network (MMST) to remove the external noise in the task of the automatic speech recognition by using the mechanism of sparse self-attention [38] and B. Jiang et al. constructed the so-called "EFFNet" model for image denoising by enhancing the transformed frequency features with dynamic hash attention [39]. Inspired by the above work, a novel image denoising method based on the complex shearlet transform and the cycle-consistent adversarial networks (CycleGAN) is developed to improve the denoising performance.

The main contribution of this research work is as follows:

Firstly, a simplified but efficient cycle-consistent adversarial network is constructed. Compared with other deep learning models, it does not need a large amount of pairwise training data with labels. So, the accuracy and robustness, stability is high.

Secondly, the image denoising is modeled to be the problem of the adversarial learn; the mapping between the noise-free image domain and the noisy image domain. As the state-of-the-art multiscale representation tool, the complex shearlet transform is employed to construct the image generator, which is able to preserve the significant and important characteristics well.

Finally, five state-of-the-art denoising methods are conducted to prove its effectiveness and accuracy. Experimental results demonstrate it produces the best denoising results both in the qualitative and quantitative analysis.

The paper is structured into several sections. Section I introduces the background of the denoising methods. Section II describes the related work on the CycleGAN and the CST. Section III presents the details of the whole proposed method. Section IV conducts the experiments and discussions. Section V finally presents the conclusion and discusses the further plan.

II. The Related Work

A. The CycleGAN

The CycleGAN model is a very typical model to deal with the problem of the image to image translation in the vison and graphics domain, whose goal is to train a useful mapping between the source domain and the target domain without the paired or aligned input-output data set.

According to [40], the principle of the CycleGAN is based on two core concepts: the basic GAN model and the Cycle Consistency Loss. The GAN is used to generate images in the target domain similar to the given training data, while the cycle consistency loss encourages the generated images to be returned to the original images in the source domain.

As shown in Fig. 1, the CycleGAN consists of two mappings functions G and F, and their associated discriminators Dx and Dy. Different from the GAN, CycleGAN contains two generators and two discriminators, where one generator converts the data from the source domain to the target domain and the other generator converts it back to the source domain. The discriminators are used to determine whether the transformed data are true or false in the two directions.

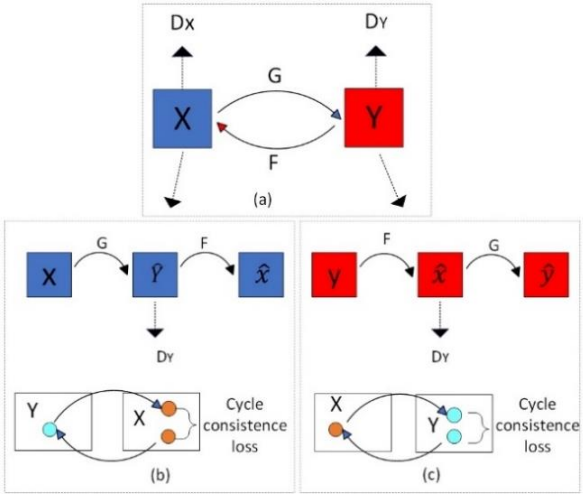

Fig. 1. The structure of the CycleGAN model.

For the training process, a generator and a discriminator network are trained separately in each domain. The purpose of the discriminator is to determine whether the generated data is realistic, while the generator is to generate a more realistic data to deceive the discriminator. The input of the generator is the data from the source domain and the output is the data from the target domain. The output of the discriminator is a probability value that indicates whether the data is real or generated.

During the training process, the generator is encouraged to generate more realistic data by calculating the difference between the output of the generator and the data in the target domain. Two cycle consistency losses are used to regularize the outputting mapping.

B. The Complex Shearlet Transform

As state-of-the-art multi-scale geometric transform tool, the complex shearlet transform is especially suitable to represent the local feature of the images by using the phase and amplitude information. It has many unique characteristics. For example, the different discrete shearlet transform, the CST is proposed with strict mathematical theory guarantee to meet the Parsval frame. Furthermore, though it has the similar property of shift invariance with the non-subsampled shearlet transform, it has the simpler implementation and higher computational efficiency. In addition, the CST has stronger direction selectivity.

Actually, the discrete implementation of the CST is realized by using the Laplace pyramid for multi-resolution analysis, and the multi-scale partition filters to get the directions. How to implement the CST is not the research hotspot in this paper, more details can be found in [41]. Fig. 2 shows an example of the CST.

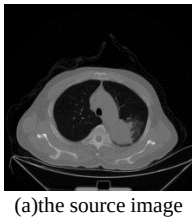

(a)the source image

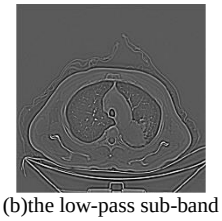

(b)the low-pass sub-band

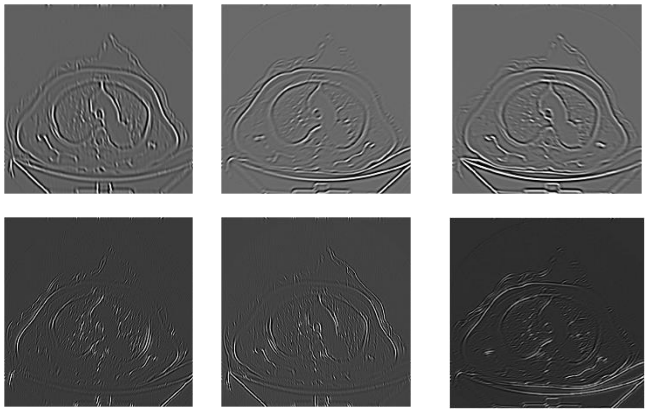

(c)the high-pass sub-bands at the first and second level

Fig. 2. An example of the CST.

III. The Proposed Method

The main purpose is to make the full use of the advantage of the CycleGAN, that is, its training does not require one-to-one image samples. Only the two types of image domains are ok. Specifically speaking, for the proposed method, it does not need the sample labels to guide the training process, but only the set of images containing noise and without noise are required. It greatly enhances the generalization and makes the network more effective to avoid the overfitting phenomena in learning the mapping from the noise-containing image domain to the noise-free image domain.

A. The Whole Process

The proposed model is shown in Fig. 3.

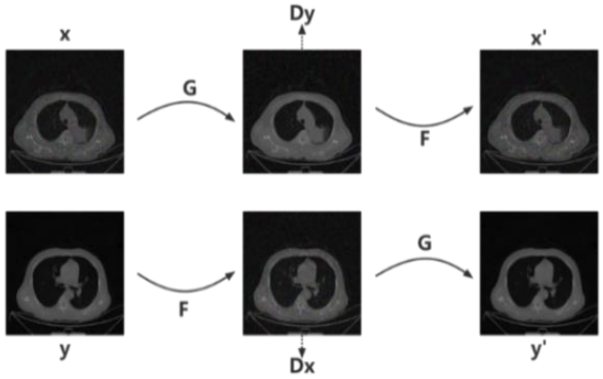

Fig. 3. The process of the proposed model.

As shown below, it mainly consists of two generators and two discriminators; X, Y is noisy images in the X and Y domain, respectively. Images in the X domain can be generated by the generator G, and then reconstructed back to X domain by generator F. Similarly, images in the Y domain can be generated by the generator F, and then reconstructed back to the Y domain by the generator G. The discriminators Dx and Dy play a discriminatory role to ensure the migration of the images.

B. The Process of Image Generation

The CycleGAN model is proposed to solve the image translation problem, so two generators are needed to realize

the transformation between two domains. However, For the image denoising problem, the aim is mainly to solve the mapping from noise-containing to noise-free without caring about the mapping from noise-free to noise-containing, so the two styles of the generators in CycleGAN are simplified in our method, and a separate noise extractor is used to realize the mutual transformation between noise-containing and noise-free images [42].

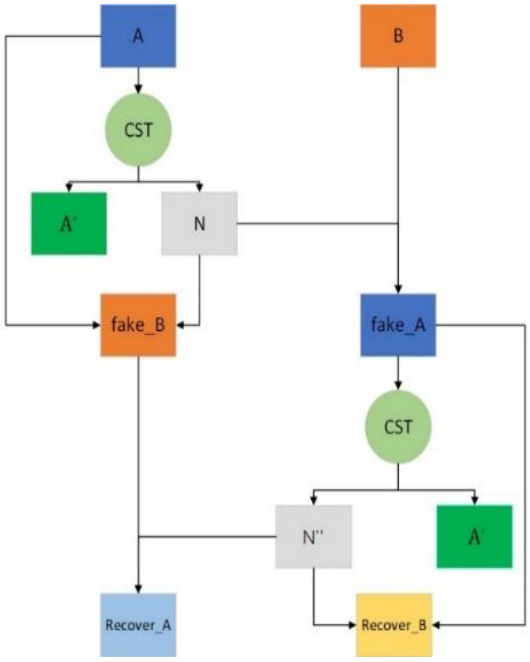

Fig. 4. The procedure of the image generation.

As shown in Fig. 4, there are six types of images involved in the generating procedure, and the CST is used to produce them to input more feature information in the training. Firstly, let A be the noisy sample image in the dataset and B be the noiseless sample; then, A is input through the CST extractor to get the noise component N, the noise image A is subtracted from the noise component N to get the denoised image fake_B, the noiseless image B is added to the noise component to get the generated noise image fake_A. The fake_A is passed through the CST noise extractor again to get the noise component N', fake_A is subtracted from the noise component N' to get the secondary noisy image. The noisy image B is added with the noise component to get the generated noisy image fake_A, the noise component N' is obtained by passing fake_A through the CST noise extractor again, the noisy image recovered_B is obtained by subtracting fake_A from the noise component N', the noisy image recovered_B is obtained by adding fake_B with the noise component N', and the noisy image recovered_A is obtained by adding fake_B with the noise component N'. recovered_A, and the noise-free sample image A is outputted by the CST noise extractor to predict the noise component in the noise-free image, and the ideal output value should be 0.

C. The Loss Function

In the proposed method, three models are needed to update the parameters, i.e. the noise extractor G, discriminator DA and discriminator DB. According to the basic CycleGAN, the loss of the two discriminators consists of the discriminant error to determine whether the image is real or the generated. And the loss of the generator is composed of three losses, i.e. the loss_GAN, loss_indentity and loss_cycle. In our method, the discriminant error is also maintained, and in order to improve the stability of the model and speed up the training, a new denoising loss (noted as loss_denoise) is added to the training of the model. More details on the calculation of the losses can be found in the following description.

1) Consistency loss is obtained from the final output images of A and the generator G, and the final output images of B and generator F. In an ideal state, the final output images between A and B should be identical, so the difference between them is used to be the consistency loss.

2) The adversarial loss is the opposite to the discriminatory loss of the discriminator, which represents the ability of fake_A and fake_B to deceive the discriminator. So, the correct judgment of the discriminator is used to be the adversarial loss.

3) The cyclic consistency loss is obtained from the images recovered_A and recovered_B generated by adding noise and removing noise from the generated images fake_A and fake_B again and the original images A and B. Recovered_A and recovered_B should be similar to A and B respectively to the maximum extent in order to ensure the noise is successfully removed without affecting other information. Therefore, the difference between them is used to be the cyclic consistency loss.

4) The denoising loss similar to it is in the general image denoising model. Thus, the difference between the noise-containing image after passing through the noise extractor and the noise-free image is used to be the denoising loss.

The calculation of the four types of losses can be divided into two categories, one is to calculate the error, and the other one is to calculate the difference between two images, which can be represented by the Mean Squared Error (MSE) and Mean Absolute Error (MAE) in the following equations.

$$MSE(y, y') = \frac{\sum_{i=1}^{n} (y, y')^2}{n} \quad (1)$$

As the calculation of the adversarial loss and the discriminator loss needs to be compared with the output of the discriminator, so y in Equation (1) is the target value with 0 or 1, y' is the output of the discriminator, and n is the number of a batch in the training, which is calculated uniformly for the output of the whole batch.

$$MAE(u, u') = \frac{\sum_{i=1}^{n} |u_i - u_i'|}{n} \quad (2)$$

For the other type of loss, it is necessary to compare the magnitude of the difference between the two images, so a pixel-by-pixel comparison is required. In Equation (2), u is the real image, u' is the generator-generated image, and n is the number of a batch in training.

After obtaining the four losses, the loss loss_G of the noise extractor model can be obtained by Equation (3) to (7).

$$Loss\_A = (loss\_indentityA + loss\_indentityB) * a \quad (3)$$

$$Loss\_B = (loss\_GANA + loss\_GANB) * b \quad (4)$$

$$Loss\_C = (loss\_cycleA + loss\_cycleB) * c \quad (5)$$

$$Loss\_D = loss\_denoise * d \quad (6)$$

$$Loss\_G = Loss\_A + Loss\_B + Loss\_C + Loss\_D \quad (7)$$

In the above equation, a, b, c and d are the weighting coefficients.

After the CST, the low-frequency sub-band images usually contain few noise components, so the loss_denoise accounts for a relatively small proportion of the loss, and it mainly relies on the consistency loss to ensure that the original image information is not lost. For high-frequency sub-band images, they contain more noise components. Thus, the loss_denoise ratio should be adjusted upward to focus on noise removal, and the ratio of the other losses should not be adjusted downward too much, ensuring that the high-frequency details of the texture in the image not be removed by any mistake.

IV. The Experiments and Discussion

A. Experiment Setting

The experimental platform is the CentOS Linux with Intel Xeon Silver and the NVIDIA Tesla P100. All the codes are implemented by the PyTorch and OpenCV.

The peak signal-to-noise ratio (PSNR), structural similarity index measure (SSIM), and edge preservation index (EPI) are used to be the performance metrics. To save space, how to compute them can be found in [43, 44].

The experiments are designed to be two parts: training the CycleGAN denoising model and verifying the effectiveness of the denoising algorithm. According to [32, 33], the deep learning-based methods outperform the traditional methods, such as the Wiener filtering, polynomial regression, or the wavelet denoising, so the proposed method is compared with five state-of-the-art denoising methods, i.e. the NSST-BM3D model [18], the FFDNet model [30], the FFCNN model [31], the GAN model [35] and the NSTBNet model [36]. The parameters, such as the size of the convolutional layer, the network depth, are set to be the same as they are reported in the corresponding literature. For the implementation of proposed model, the basic structure of the CycleGAN is used get the best performance by tuning the parameters according to [40].

All the images can be downloaded from the public data set LIDC-IDRI [45], and 5000 images are selected in the experiments. All of them are added the 10%, 15%, 20%, 25%, and 30% Poisson noise [46].

B. Results and Discussion

Table I shows the average PSNR values obtained by the different methods under the five noise levels of 10%, 15%, 20%, 25%, and 30%. It can be seen that the proposed method gets the best value. Compared with NSST-BM3D, FFCNN, and FFDNet, the improvements are more obvious when the noise is at the higher level. Compared with NSTBNet and GAN, the PSNR values are also higher.

TABLE I. The PSNR Value of Different Methods

Level	NSST-BM3D	FFCNN	FFDNet	NSTBNet	GAN	CycleGAN
10%	29.84	30.02	30.10	30.13	30.20	30.38
15%	28.01	28.18	28.29	28.36	28.39	28.63
20%	26.15	26.22	26.30	26.35	26.38	26.44
25%	25.12	25.24	25.28	25.30	25.31	25.44
30%	23.43	23.51	23.64	23.66	23.71	23.95

TABLE II. The SSIM Value of Different Methods

Level	NSST-BM3D	FFCNN	FFDNet	NSTBNet	GAN	CycleGAN
10%	0.872	0.875	0.875	0.882	0.875	0.891
15%	0.801	0.796	0.806	0.813	0.807	0.876
20%	0.762	0.763	0.776	0.783	0.784	0.794
25%	0.706	0.723	0.724	0.735	0.740	0.755
30%	0.663	0.703	0.710	0.715	0.719	0.723

TABLE III. The EPI Value of Different Methods

Level	NSST-BM3D	FFCNN	FFDNet	NSTBNet	GAN	CycleGAN
10%	0.94	0.95	0.95	0.96	0.97	0.98
15%	0.90	0.89	0.91	0.92	0.91	0.94
20%	0.83	0.846	0.86	0.87	0.87	0.89
25%	0.80	0.82	0.83	0.85	0.84	0.86
30%	0.70	0.71	0.73	0.75	0.77	0.81

Table II and Table III show the average SSIM and EPI values of different methods at the five different noise levels, respectively. The CycleGAN value is higher than that for the other methods. When the noise level increases, its advantages will slowly manifest, especially when the noise level is 20% and 25%, the SSIM is significantly higher than the other methods and when the noise level is 20%, the EPI get the best value.

The reason is that during the training process, the denoising extractor in the proposed method makes full use of the CST features via the low-pass and high-pass sub-bands coefficients. The consideration of the geometric and structural features of the source can be well maintained in the final result and guarantee the good value of the SSIM and EPI.

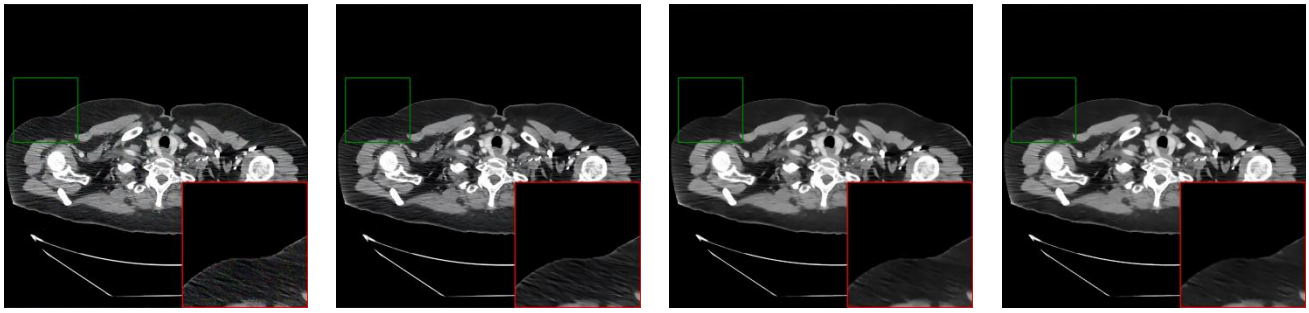

(a) The noisy image (b) The ground truth (c) NSST-BM3D (d) FFCNN

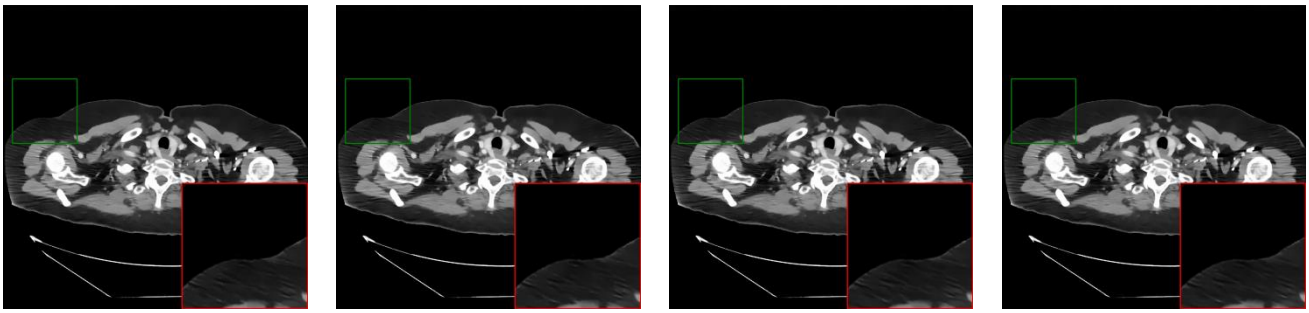

(e) FFDNet (f) NSTBNet (g) GAN (h) CycleGAN

Fig. 5. The denoising results at the 10% noise level.

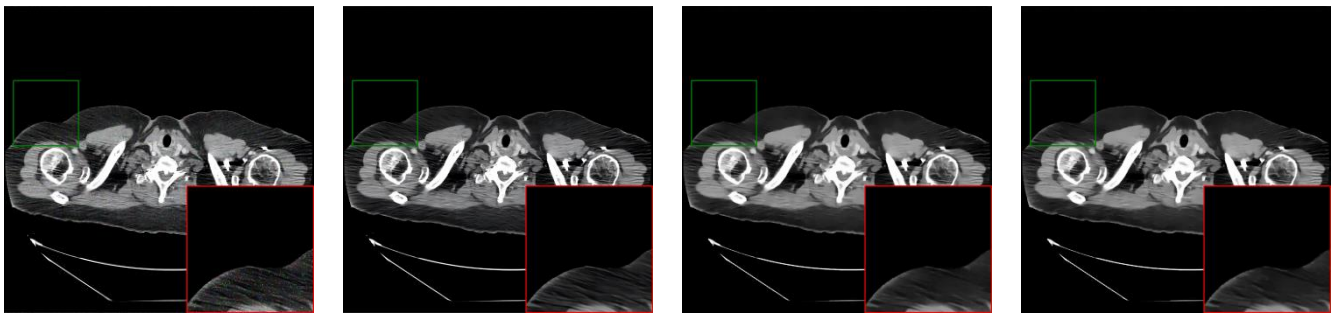

(a) The noisy image (b) The ground truth (c) NSST-BM3D (d) FFCNN

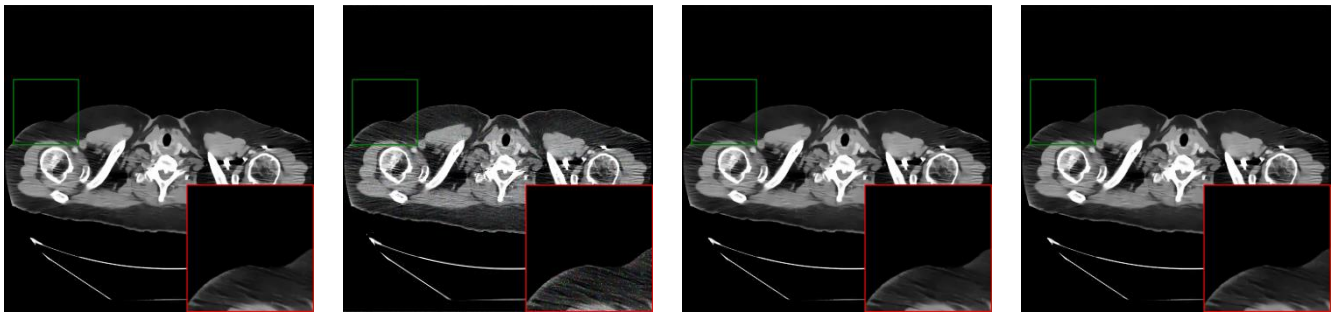

(e) FFDNet (f) NSTBNet (g) GAN (h) CycleGAN

Fig. 6. The denoising results at the 15% noise level.

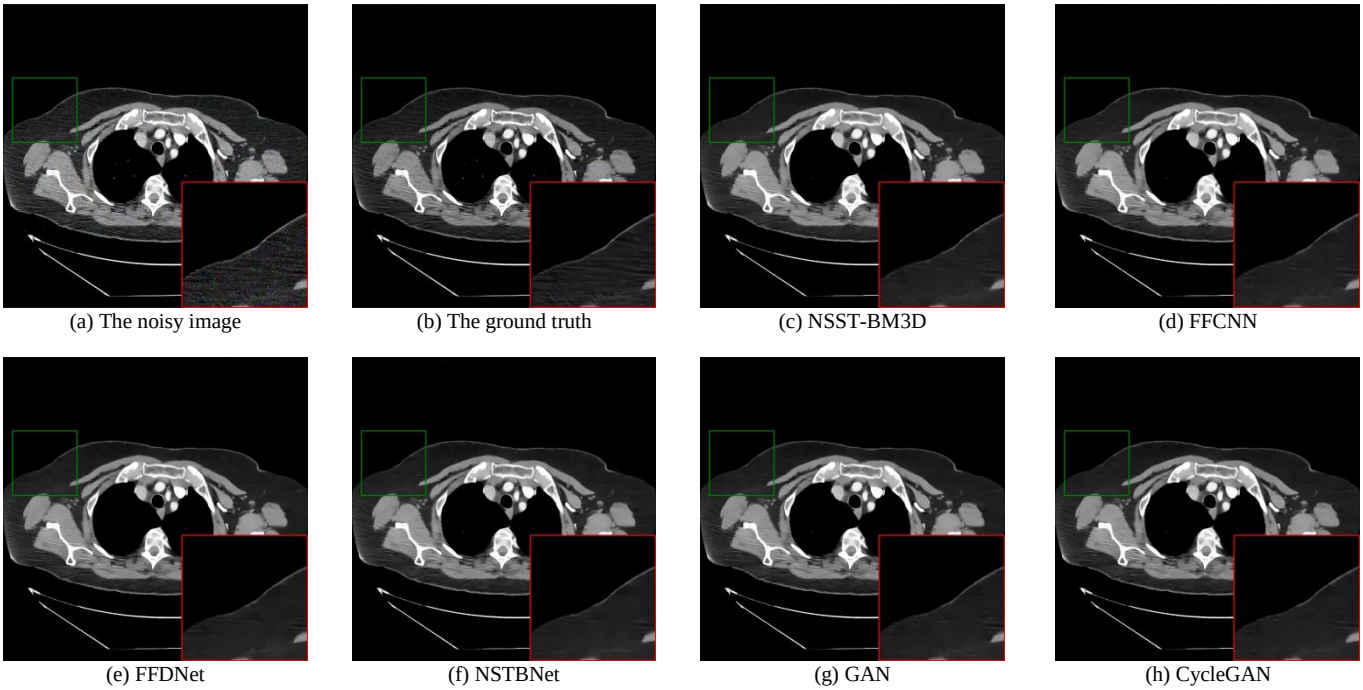

(a) The noisy image (b) The ground truth (c) NSST-BM3D (d) FFCNN

(e) FFDNet (f) NSTBNet (g) GAN (h) CycleGAN

Fig. 7. The denoising results at the 20% noise level.

In Fig. 5 to Fig. 7, the visual results of the different methods are shown. Due to space limitations, only three groups of the experimental images are presented. The area marked by the red squares is enlarged at the same location. Compared with the ground truth and noisy images, the results of the CycleGAN method are more clear and they perform better in maintaining more feature details than other methods. According to the enlarged area, the details can be compared. The edge part of CycleGAN denoising image is more smooth and clearer, and the detail part is almost equivalent to it is in the ground truth.

Medical image denoising is very important in kinds of medical imaging processing tasks. After the optimization, the proposed model can be applied into the object detection, segmentation, and classification tasks enabled by the denoising techniques mentioned in this paper.

V. Conclusion

An effective medical image denoising method based on the improved CycleGAN model and the complex shearlet transform is proposed. The main idea is to use the multi-scale decomposition property of the CST and the principle of the recurrent learning of the GAN. The advantages mainly locate at the strong ability of the extracting the important structure and edge information of the noisy images and training an effective cycle GAN model. Compared with five state-of-the-art denoising methods on the open dataset, the validity and accuracy are fully demonstrated.

In future, we will discuss with some medical experts to implement more experiments on the data from different imaging modalities, such as the MRI, PET and Ultrasound, and consider their feedback to validate the effectiveness.

Acknowledgment

This study is supported by: A project ZR2021MF017 supported by Shandong Provincial Natural Science Foundation; a project 2023RKY01015 supported by the Key R&D Program of Shandong Province, China; a project ZR2020MF147 supported by Shandong Provincial Natural Science Foundation.

References

[1] M. Diwakar, M. Kumar, “A review on CT image noise and its denoising,” Biomedical Signal Processing and Control, vol. 42, pp.73-88, April 2018.

[2] J. Gong, J. Guan, C. Liu and J. Qi, “PET image denoising using a deep neural network through fine tuning,” IEEE Transactions on Radiation and Plasma Medical Sciences, vol. 3, no. 2, pp. 153-161, March 2019.

[3] J. Huang, L. Wang, M. Tahir, T. Cheng, X. Guo, Y. Wang and C. Liu, “The Effective 3D MRI reconstruction method driven by the fusion strategy in NSST domain,” International Journal of Advanced Computer Science and Applications(IJACSA), vol.14, no.4, pp.709-715, April 2023.

[4] E. Yahaghi, M. Mirzapour, A. Movafeghi and B. Rokrok. “Interlaced bilateral filtering and wavelet thresholding for flaw detection in the radiography of weldment,” The European Physical Journal Plus, vol.135, pp.42-52, January 2020.

[5] F. Ashouri, and M. R. Eslahchi, “A new PDE learning model for image denoising,” Neural Computing and Applications, pp. 8551-8574, March 2022.

[6] A. Vyas, J. Paik, “Applications of multiscale transforms to image denoising: Survey,” 2018 International Conference on Electronics, Information, and Communication (ICEIC), Honolulu, HI, USA, pp. 1-3, January 2018.

[7] S. Roy, S. Imran Hossain, M. Akhand and K. Murase, “A robust system for noisy image classification combining denoising autoencoder and convolutional neural network,” International Journal of Advanced Computer Science and Applications(IJACSA), vol. 9, no.1, pp.224-235, September 2018.

[8] S. Sagheer, and S. George, "A review on medical image denoising algorithms," Biomedical Signal Processing and Control, vol. 61, pp.102036, June 2020.

[9] B. Zhang, J. Allebach, "Adaptive bilateral filter for sharpness enhancement and noise removal," IEEE Transactions on Image Processing, vol. 17, no. 5, pp. 664-678, May 2008.

[10] Y. Wu, S. Li. "A novel fusion paradigm for multi-channel image denoising," Information Fusion, vol.77, pp.62-69, August 2021.

[11] Y. Do, Y. Cho, S H. Kang and Y. Lee, "Optimization of block-matching and 3D filtering (BM3D) algorithm in brain SPECT imaging using fan beam collimator: Phantom study," Nuclear Engineering and Technology, vol. 54, no. 9, pp.3403-3414, 2022.

[12] H. Singh, S. Kommuri, A. Kumar and V. Bajaj, "A new technique for guided filter based image denoising using modified cuckoo search optimization," Expert Systems with Applications, vol. 176, pp.114884, August 2021.

[13] G. Gilboa, N. Sochen and Y. Zeevi, "Image enhancement and denoising by complex diffusion processes," IEEE Transactions on Pattern Analysis and Machine Intelligence, vol. 26, no. 8, pp. 1020-1036, August 2004.

[14] K. Allard, G. Chen and M. Maggioni, "Multi-scale geometric methods for data sets II: geometric multi-resolution analysis," Applied and Computational Harmonic Analysis, vol. 32, no. 3, pp. 435-462, May 2012.

[15] Q. Ren, B. Zhou, L. Tian and W. Guo, "Detection of COVID-19 with CT images using hybrid complex shearlet scattering networks," IEEE Journal of Biomedical and Health Informatics, vol. 26, no. 1, pp. 194-205, January 2022.

[16] A. Halidou, Y. Mohamadou, A. Ari and E. Zacko, "Review of wavelet denoising algorithms," Multimedia Tools and Applications , https://doi.org/10.1007/s11042-023-15127-0, April 2023

[17] P. S. Negi, and D. Labate, "3-D discrete shearlet transform and video processing," IEEE Transactions on Image Processing, vol. 21, no. 6, pp. 2944-2954, June 2012.

[18] X. He, C. Wang, R. Zheng, Z. Sun and X. Li, "GPR image denoising with NSST-UNet and an improved BM3D," Digital Signal Processing, vol. 123, pp.103402, April 2022.

[19] M. Hu, B. Sun, X. Kang and S. Li, "Multiscale structural feature transform for multi-modal image matching," Information Fusion, vol.95, pp.341-354, July 2023.

[20] Y. Liu, S. Liu and Z. Wang, "A general framework for image fusion based on multi-scale transform and sparse representation," Information Fusion, vol. 24, no. 4, pp. 147-164, July 2015.

[21] M. Hashemi, S. Beheshti, "Adaptive bayesian denoising for general gaussian distributed signals," IEEE Transactions on Signal Processing, vol. 62, no. 5, pp. 1147-1156, March 2014.

[22] L Wang, B Li and L Tian, "EGGDD: An explicit dependency model for multi-modal medical image fusion in shift-invariant shearlet transform domain," Information Fusion, vol. 19, pp. 29-37, September 2014.

[23] M. M. Ichir, A. Mohammad-Djafari, "Hidden markov models for wavelet-based blind source separation," IEEE Transactions on Image Processing, vol. 15, no. 7, pp. 1887-1899, July 2006.

[24] X. Wang, R. Song, Z. Mu and C. Song, "An image NSCT-HMT model based on copula entropy multivariate Gaussian scale mixtures," Knowledge-Based Systems, vol. 193, pp.105387, April 2020.

[25] X. Wang, Y. Liu and H. Yang, "Image denoising in extended shearlet domain using hidden markov tree models," Digital Signal Processing, vol. 30, pp. 202-113, July 2014.

[26] P. Gupta, A. Krishna Moorthy, R. Soundararajan and A. Bovik, "Generalized gaussian scale mixtures: A model for wavelet coefficients of natural images," Signal Processing: Image Communication, vol. 66, pp. 87-94, August 2018.

[27] A. Kalluvila, "Super-Resolution of Brain MRI via U-Net architecture," International Journal of Advanced Computer Science and Applications, vol.14, no.5, pp.26-31, May 2023.

[28] A. Saif, E. Wollega and S. Kalevela, "Spatio-Temporal features based human action recognition using convolutional long short-term deep neural network," International Journal of Advanced Computer Science and Applications(IJACSA), vol.14, no.5, pp.1-15, May 2023.

[29] Y Xia, J. Dong, D. Li, K. Li, J. Nan and R. Xu, "An adaptive channel selection and graph resnet based algorithm for motor imagery classification," International Journal of Advanced Computer Science and Applications(IJACSA), vol.14, no.5, pp.241-248, May 2023.

[30] K. Zhang, W. Zuo and W. Zhang. "FFDNet: Toward a fast and flexible solution for CNN-based image denoising," IEEE Transactions on Image Processing, vol.27, no.9, pp.4608-4622, September 2018.

[31] W. Li, H. Liu and J. Wang, "A deep learning method for denoising based on a fast and flexible convolutional neural network," IEEE Transactions on Geoscience and Remote Sensing, vol.60, pp.1-13, April 2021.

[32] K. Zhang, W. Zuo, Y. Chen, D. Meng and L. Zhang. "Beyond a gaussian denoiser: Residual learning of deep CNN for image denoising," IEEE Transactions on Image Processing, vol.26, no.7, pp.3142-3155, July 2017.

[33] R. Thakur, R. Yadav and L. Gupta, "State-of-art analysis of image denoising methods using convolutional neural networks," IET Image Processing, vol.13, no.13, pp.2367-2380. November 2019.

[34] A. Creswell and A. Bharath, "denoising adversarial autoencoders," IEEE Transactions on Neural Networks and Learning Systems, vol. 30, no. 4, pp. 968-984, April 2019.

[35] M. B. de Almeida, L. F. Alves Pereira, T. I. Ren, G. D. C. Cavalcanti and J. Sijbers, "The gated recurrent conditional generative adversarial network (GRC-GAN): application to denoising of low-dose CT images," 34th SIBGRAPI Conference on Graphics, Patterns and Images (SIBGRAPI), Gramado, Rio Grande do Sul, Brazil, pp. 129-135, October 2021.

[36] Z. Lyu, Y. Chen, Y. Hou and C. Zhang, "NSTBNet: toward a non-subsampled shearlet transform for broad convolutional neural network image denoising," Digital Signal Processing, vol.123, pp.103407, April 2022.

[37] C. Gu, H. Gao, "Combining GAN and LSTM models for 3D reconstruction of lung tumors from CT scans," International Journal of Advanced Computer Science and Applications(IJACSA), vol.14, no.5, pp.378-388, May 2023.

[38] Q. Song, B. Sun and S. Li, "Multimodal sparse transformer network for audio-visual speech recognition," IEEE Transactions on Neural Networks and Learning Systems, pp.1-11, April 2022.

[39] B. Jiang, J. Li, H. Li, R. Li, D. Zhang and G. Lu, "Enhanced frequency fusion network with dynamic hash attention for image denoising," Information Fusion, vol. 92, pp.420-434, April 2023.

[40] J. Zhu, T. Park, P. Isola and A. Efros, "Unpaired image-to-image translation using cycle-consistent adversarial networks," IEEE International Conference on Computer Vision (ICCV), Venice, Italy, pp.2242-2251, October 2017.

[41] M. Wang, C. Sun and A. Sowmya, "Complex shearlets and rotary phase congruence tensor for corner detection," Pattern Recognition, vol.128, pp.108606, August 2022.

[42] I. Anokhin, K. Demochkin, T. Khakhulin, G. Sterkin, V. Lempitsky and D. Korzhenkov, "Image generators with conditionally-independent pixel synthesis," The IEEE/CVF Conference on Computer Vision and Pattern Recognition, pp.14278-14287, June 2021.

[43] E. Reehorst and P. Schniter, "Regularization by denoising: clarifications and new interpretations," IEEE Transactions on Computational Imaging, vol.5, no.1, pp.52-67, March 2019.

[44] K. Egiazarian, M. Ponomarenko, V. Lukin and O. Leremiev, "Statistical evaluation of visual quality metrics for image denoising," IEEE International Conference on Acoustics, Speech and Signal Processing (ICASSP), pp.6752-6756, November 2018.

[45] S. Kollem, K. Reddy and D. Rao, "Improved partial differential equation-based total variation approach to non-subsampled contourlet transform for medical image denoising," Multimedia Tools and Applications, pp.2663-2689, January 2021.

[46] R. Harper, S. Flammia and J. Wallman, "Efficient learning of quantum noise," Nature Physics, vol.16, pp.1184-1188, August 2020.